Prepared for submission to JCAP

Model Selection Using Cosmic Chronometers with Gaussian Processes

Fulvio Melia[1,3] **and Manoj K. Yennapureddy**[2]

[3]Department of Physics, the Applied Math Program, and Steward Observatory,
The University of Arizona, Tucson, AZ 85721

[2]Department of Physics, The University of Arizona, Tucson, AZ 85721

E-mail: fmelia@email.arizona.edu; manojy@email.arizona.edu

Abstract. The use of Gaussian Processes with a measurement of the cosmic expansion rate based solely on the observation of cosmic chronometers provides a completely cosmology-independent reconstruction of the Hubble constant $H(z)$ suitable for testing different models. The corresponding dispersion σ_H is smaller than $\sim 9\%$ over the entire redshift range ($0 \lesssim z \lesssim 2$) of the observations, rivaling many kinds of cosmological measurements available today. We use the reconstructed $H(z)$ function to test six different cosmologies, and show that it favours the $R_\mathrm{h} = ct$ universe, which has only one free parameter (i.e., H_0) over other models, including *Planck* ΛCDM. The parameters of the standard model may be re-optimized to improve the fits to the reconstructed $H(z)$ function, but the results have smaller p-values than one finds with $R_\mathrm{h} = ct$.

[1]John Woodruff Simpson Fellow.

Contents

1 Introduction

Two recent developments have made it possible for us to measure the Hubble constant $H(z)$ without having to assume any particular model, thereby providing a truly model-independent probe of the expansion dynamics. The first of these is the development of a technique used to measure the differential ages of adjacent galaxies out to a redshift $z \sim 2$ [1, 2]. The second is the introduction of Gaussian Processes to the analysis of the variables, such as $H(z)$, allowing us to reconstruct their functional form without having to assume any *a priori* parametric dependence on redshift or other theoretical constraints [3–5].

Galaxies evolving passively over a time much longer than their age difference allow us to measure the expansion rate $H(z)$ solely as a function of the redshift-time derivative dz/dt. These ages are inferred from the observed 4,000 Å break in the passively evolving spectra, based on our understanding that, for old stars, this break is due to metal absorption lines whose amplitude scales linearly with stellar age. So when the metallicity of these stars is known, the age difference of two adjacent galaxies is proportional to the difference of their 4,000 Å amplitudes [2]. In previous applications [2, 6–8], these cosmic chronometers (as they are called) have been used successfully to compare the predictions of various cosmological models, such as the standard model ΛCDM and another Friedmann-Robertson-Walker cosmology known as the $R_{\rm h} = ct$ universe [9–11]. Quite surprisingly, a constant expansion rate is preferred when the Hubble constant $H(z)$ is measured using cosmic chronometers on their own, without the bias introduced via the inclusion of other data at low z, such as the measurement of H_0 using Cepheid variables, whose peculiar velocities associated with the influence of a local "Hubble Bubble" are comparable to those in the Hubble flow [12]. First attempts at identifying the distance beyond which the Hubble flow dominates noticeably over local, peculiar velocities yielded an estimate of $\sim 80h^{-1}$ Mpc, where h is the Hubble constant scaled to 100 km s^{-1} Mpc^{-1} [13]. More recent studies [14] of the local expansion rate have found a significant local under-density that persists out to ~ 300 Mpc, corresponding to a redshift $z \sim 0.07$ (see also ref. [15]). This effect may partly be the source of tension between cosmological parameters optimized at low redshifts compared to the values obtained by *Planck*. Instead, the expansion rate measured with cosmic chronometers appears to favour the $R_{\rm h} = ct$ model, in which the Universe expands at a constant rate.

This situation clearly calls for more in-depth analysis of the cosmic chronometer measurements, preferably using several different approaches for model selection. Our goal in this paper is to follow an alternative means of using cosmic chronometers to comparatively test these cosmologies. The use of Gaussian Processes to reconstruct $H(z)$ avoids the need of "fitting" the data with pre-determined parametric functions. This non-parametric technique for reconstructing the expansion history is a fully Bayesian approach for smoothing data. The procedure results not only in a truly model-independent determination of $H(z)$ as a function of z, but the associated errors reconstructed along with the function itself strike a balance between very smooth and rapidly oscillating variations (see, e.g., ref. [5]). Having said this, an important caveat to consider along with the results presented later in this paper is that the use of Gaussian Processes necessitates the adoption of two hyperparameters whose values are not known a priori. As discussed in greater detail in § 2 below, the common approach is to train them by maximizing the likelihood that the reconstruction matches the measured values at the data points themselves. Nonetheless, this choice of parameters affects the smoothness of the function and its errors.

In § 2 of this paper, we describe the calculation of $H(z)$ in more detail and use Gaussian Processes to "measure" this quantity out to a redshift ~ 2. We then introduce the six models we will test using this metric, and carry out the comparative analysis in § 3. Finally, we will discuss our results and provide our conclusions in § 4.

2 Reconstructing $H(z)$

In recent years, several kinds of measurement of $H(z)$ have been used to optimize the parameters in ΛCDM. In some cases [7, 8], they have also been used to compare the predictions of the standard model with those of another Friedmann-Robertson-Walker (FRW) cosmology known as the $R_{\rm h} = ct$ universe [9–11, 16, 17]. But one must be wary of combining measurements of $H(z)$ using different techniques because not all of these approaches are truly model independent. For example, measurements based on the identification of baryon acoustic oscillations (BAO) and the Alcock-Paczyński distortion from galaxy clustering depend on how 'standard rulers' evolve with redshift, rather than how cosmic time changes with z (see, e.g., ref. [18]). The values of $H(z)$ measured using these different approaches are sometimes merged together to form an overall $H(z)$ versus z diagram, but the BAO approach must necessarily adopt a particular cosmology and is therefore model-dependent. Up to this point, observations based on the cosmic chronometer idea are the only ones we are aware of that do not rely on the assumption of a particular cosmology, so they are suitable for testing and comparing different models. As we explain below, however, there is a lingering concern regarding whether or not the assumption of a single, dominant bout of star formation is valid in these galaxies, and the resolution to this question may depend on the expansion dynamics associated with each particular model.

2.1 Cosmic Chronometers

The cosmic chronometer approach is based on the notion that the expansion rate $H(z)$ may be measured using solely the redshift-time derivative dz/dt between galaxies evolving passively over a time much longer than their age difference [1]. These massive ($\gtrsim 10^{11}\ M_\odot$) early-type galaxies are thought to have formed $\gtrsim 90\%$ of their stellar mass at $z > 2-3$, over a period of only $\sim 0.1-0.3$ Gyr, when the Universe was only ~ 4 Gyr old. A more recent study of early star formation in these galaxies, however, raises some doubt about whether or not a

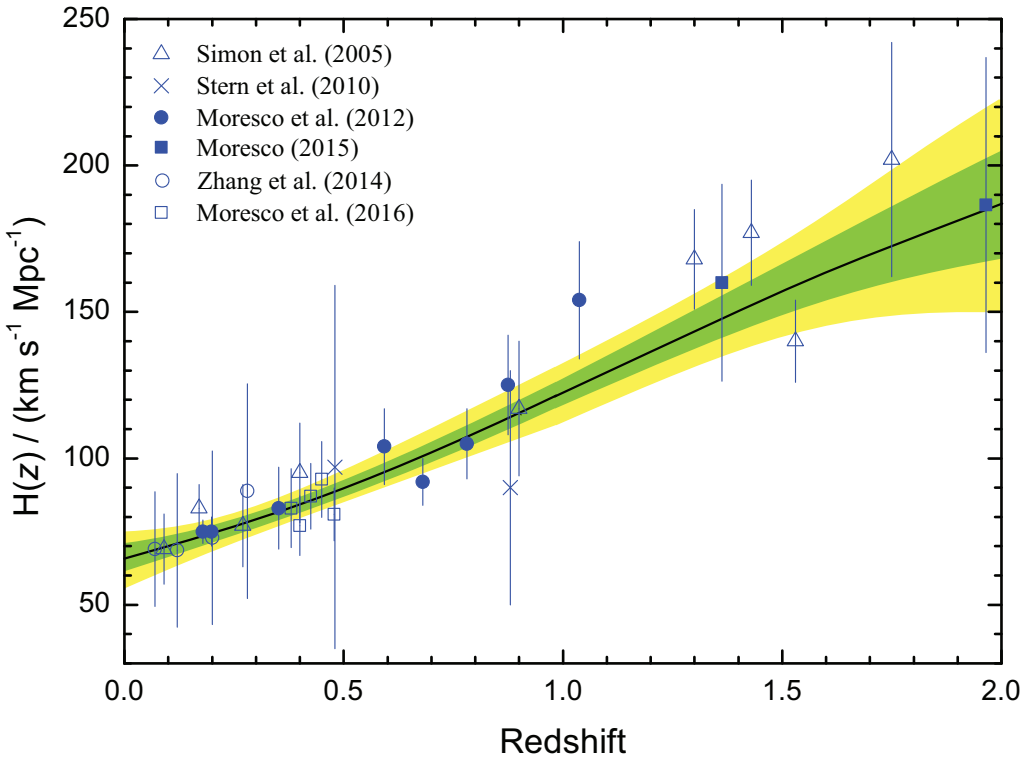

Figure 1. Thirty model-independent measurements of $H(z)$ versus z with error bars [2, 6, 20–23]. Note that these are total errors, which include both statistical and systematic contributions (see, e.g., refs. [24, 25]). Also shown here is the function $H(z)$ reconstructed with Gaussian Processes (solid black). The green and yellow shaded regions represent the 1σ and 2σ confidence regions, respectively, of the reconstruction.

single bout of star formation can fully account for the observed stellar population [25]. In this paper, we will adopt the conventional view that these galaxies experienced only minor subsequent episodes of star formation, and are thus the oldest objects at all redshifts [19], though our analysis will need to be updated when these issues are better understood. So, for example, the stellar population in such a galaxy at $z \sim 1$ (i.e., when the Universe was ~ 7 Gyr old) formed during the first $\sim 2-10\%$ of its evolution. And since one measures only the local difference in redshift between these galaxies, one avoids the need of pre-assuming a cosmological model, which constitutes a powerful discriminant for testing different expansion scenarios. The latest compilation using this approach includes 30 measurements of $H(z)$ over the redshift range $0 \lesssim z \lesssim 2$ [2].

These measurements are based on the observed 4,000 Å break in the passively evolving galaxy spectra. For old stars, this break is a discontinuity in the spectral continuum due to metal absorption lines whose amplitude scales linearly with the stellar age and metal abundance [2]. When the metallicity of these stars is known, one can measure the age difference Δt of two adjacent galaxies in proportion to the difference of their 4,000 Å amplitudes. The metallicity determines the slope of this relation. And introducing the redshift difference Δz

of these galaxies, one can then determine the Hubble constant using the simple relation

$$H(z) = -\frac{1}{(1+z)}\,\frac{dz}{dt} \approx -\frac{1}{(1+z)}\,\frac{\Delta z}{\Delta t}\,. \tag{2.1}$$

A caveat with this procedure, however, is that several factors may limit the accuracy with which the differential age of these systems is measured. Nonetheless, extensive tests [2] have demonstrated that the 4,000 Å feature is mostly dependent on the age and metallicity of the host galaxies, relying only weakly on the star formation history, their initial mass function, along with possible progenitor biases, and (the so-called) α-enhancement. These early, passive galaxies apparently have higher ratios of α elements to iron than the Milky Way. There may also be a progenitor bias due to an evolution in the mean redshift of galaxy formation as a function of redshift.

The tests that have been conducted to this point reveal that only an uncertainty in the metallicity contributes a systematic error $\sigma_{\rm sys}$ comparable to the statistical errors in the sample. The progenitor bias contributes at most only a few percent to $\sigma_{\rm sys}$, and the initial mass function has no impact. Using a Chabrier or Salpeter initial mass function for all reasonable metallicities produces a difference of less than 0.3% between the 4,000 Å amplitudes estimated for a single stellar population. The difference is less than 0.2% for solar metallicity [2]. Likewise, the α-enhancement produces an average difference in the 4,000 Å amplitudes of only $\sim 0.5\%$.

Simulations have also shown that variations in the assumed star forming rate may produce $\lesssim 13\%$ errors in the measured value of Δz from measurements of the 4,000 Å amplitudes [2]. All these effects together contribute an overall error of about 20% to Δz, and hence the inferred value of $H(z)$. The 30 measurements of $H(z)$ based on the cosmic chronometer approach are shown in figure 1 [2, 6, 20–23]. Also shown in this figure is the function $H(z)$ reconstructed from the cosmic chronometer data using Gaussian Processes, along with the 1σ and 2σ confidence regions, which we shall discuss shortly.

Before introducing the models, however, we address an issue with the data illustrated in figure 1 that has raised some concern recently regarding whether or not the associated errors are being over-estimated (see, e.g., refs. [12, 25]). The dispersions shown here are calculated in quadrature from the statistical ($\sigma_{\rm stat}$) and systematic ($\sigma_{\rm sys}$) errors, the latter of which are assumed to be uncorrelated. But this assumption may not be valid, given that some contributions to $\sigma_{\rm sys}$, e.g., the metallicity variations with redshift, are not truly random [25]. It is safe to say that, at best, $\sigma_{\rm sys}$ may have both correlated and uncorrelated components, in which case, the errors shown in figure 1 are too large. One can see this directly by comparing the published errors with the deviations of the data relative to the reconstructed $H(z)$ function, and from the fact that the reduced χ^2 is notably smaller than one ($\chi^2_{\rm dof} \sim 0.52$).

To examine the impact of this error over-estimation on model selection, in this paper we will therefore also consider a modified set of data extracted from the observations shown in figure 1 but with reduced dispersions. The ideal way to reduce the errors would be to deduce the fraction f_s representing the degree of correlation in the systematic errors with which one would then estimate the 'true' error as

$$\sigma(z_i) = \sqrt{\sigma_{\rm stat}(z_i)^2 + f_s\,\sigma_{\rm sys}(z_i)^2}\,. \tag{2.2}$$

Presumably, $f_s = 0$ corresponds to the systematic errors being fully correlated, and $f_s = 1$ totally random. As of now, however, there are several limitations that prevent us from

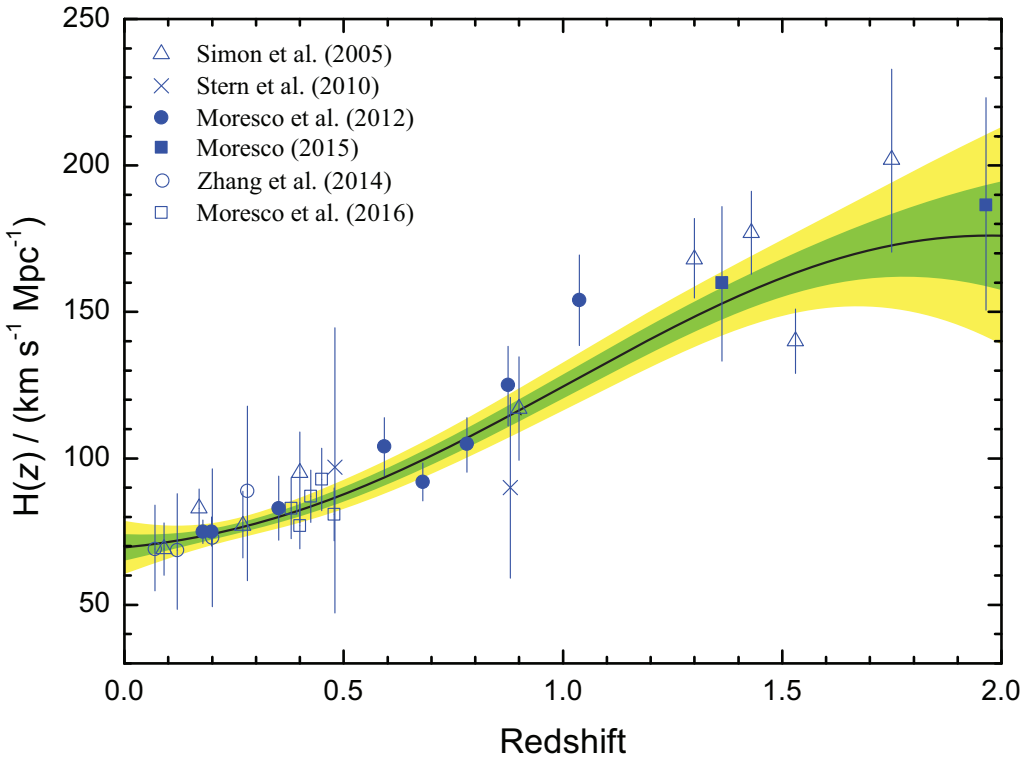

Figure 2. Same as figure 1, except that the error bars have here been reduced by an average of 25%. This modification allows a reasonable cosmological model, such as ΛCDM, to fit the data with a reduced $\chi^2_{\rm dof} \approx 1$ [12]. Also shown here is the function $H(z)$ reconstructed with Gaussian Processes (solid black). The green and yellow shaded regions represent the 1σ and 2σ confidence regions, respectively, of the reconstruction.

using this approach. The first is that we do not know f_s a priori, nor whether this is even independent of redshift. Second, of the 30 data points shown in figure 1, only 17 have published values of $\sigma_{\rm stat}$ and $\sigma_{\rm sys}$. We have attempted to reconstruct the $H(z)$ function using only this reduced set of measurements, but the Gaussian-process approach is unstable due to the sparseness of the data, producing unphysical oscillations with redshift. For now, we shall instead follow the simpler suggestion described in ref. [12], based on the idea that if correctly estimated, a reasonable model for the data in figure 1 (say, ΛCDM) should fit these measurements with a reduced $\chi^2_{\rm dof}$ approximately equal to one. Wei et al. [12] found that to attain this goal, the errors shown in figure 1 must be reduced, on average, by about 25%. The $H(z)$ data with their modified error bars are shown in figure 2, together with the reconstructed $H(z)$ function based on these reduced dispersions.

2.2 Gaussian Processes

The principal benefit of using the Gaussian Processes (GP) approach [5] is that it avoids having to assume a parametric form of the function representing the data based on particular models that may, or may not, be reasonable representations of the true redshift-dependence of the measurements. A complete description of this method has been provided in ref. [5], and a catalog of related algorithms may be downloaded from a website maintained by these

authors.[1]

Gaussian Processes can model a function f(x) rigorously without assuming any prior parametric form. One assumes that the n observations of a data set y=$\{y_1, y_2, ..., y_n\}$ were sampled from a multivariate Gaussian distribution, which then allows these data to be partnered with Gaussian Processes (GP). Most often, the mean of this partner GP is assumed to be zero. But though modeling the data using Gaussian Processes is straightforward, there are nonetheless two possible areas of ambiguity with this technique, so we highlight these here and describe steps we have taken to ensure that the outcome of our reconstruction is not heavily biased by our choice of GP components. One of these has to do with the fact that the values of the function evaluated at different points x_1 and x_2 are not independent of each other. As such, one introduces a covariance function $k(x_1, x_2)$ to handle the linkage between neighboring points, though the form of $k(x_1, x_2)$ is not unique or well known. In principle, there is a broad range of such covariance functions, and while it makes sense to pick one that depends only on the distance between different data points, this is actually not required. It is common in this type of work to select a squared exponential function for this purpose,

$$k(x_1, x_2) = \sigma_f^2 \exp\left(-\frac{(x_1 - x_2)^2}{2l^2}\right) , \tag{2.3}$$

simply because it is infinitely differentiable and useful for reconstructing also the derivative of a function that represents the data. In contrast to actual parameters, the so-called hyperparameters σ_f and l do not specify the form of the function, only its "bumpiness." The characteristic length l represents a distance in x over which the reconstructed function varies significantly, while the signal variance σ_f scales this dependence in the ordinate direction. The covariance matrix obtained using Equation (2.3) for $\{x_1, x_2, ...x_n\}$ observation points is

$$K = \begin{bmatrix} k(x_1,x_1) & k(x_1,x_2) & ..... & k(x_1,x_n) \\ k(x_2,x_1) & k(x_2,x_2) & ..... & k(x_2,x_n) \\ ..... & ..... & ..... & ..... \\ k(x_n,x_1) & k(x_n,x_2) & ..... & k(x_n,x_n) \end{bmatrix} . \tag{2.4}$$

For a new observation point x_*, one also needs the vector

$$K_* \equiv \begin{bmatrix} k(x_*,x_1) & k(x_*,x_2) & ..... & k(x_*,x_n) \end{bmatrix} , \tag{2.5}$$

and the point $K_{**} \equiv k(x_*, x_*)$. As we have pointed out, the data may be represented as a sample from a multivariate GP, such that

$$\begin{bmatrix} y \\ y_* \end{bmatrix} = N\left(0, \begin{bmatrix} K & K_*^T \\ K_* & K_{**} \end{bmatrix}\right) . \tag{2.6}$$

In obtaining this, one must maximize the conditional probability

$$p(y_*|y) \sim N(K_* K^{-1} y, K_{**} - K_* K^{-1} K_*^T) . \tag{2.7}$$

The mean of the distribution is an estimate of y_*, which is given as

$$\mu(y_*) = K_* K^{-1} y , \tag{2.8}$$

[1] http://www.acgc.uct.ac.za/∼seikel/GAPP/index.html

and the uncertainty of the estimate is given as

$$\mathrm{var}(y_*) = K_{**} - K_* K^{-1} K_*^T \ . \tag{2.9}$$

All of the results discussed in this paper, particularly those shown in figs. 1-6, are based on the use of the kernel given in Equation (2.3). However, to ensure that this choice of covariance function is not unduly affecting our model selection, we also carry out a parallel set of simulations in the Appendix based on the use of a very different kind of kernel known as a Matérn covariance function, specifically the one called Matérn92 [5]. As described in the Appendix, the choice of kernel may change the p-values by a few points, but the outcome of model selection based on this approach is not changed qualitatively. The rank ordering of models we consider here (see below) appears to be unaffected by the choice of covariance function.

A second possible area of ambiguity has to do with the values of the hyperparameters themselves. The common approach followed in this context is to train them by maximizing the likelihood that the reconstructed function has the measured values at the data points x_i. Of course, for a purely Bayesian analysis, one should marginalize over the hyperparameters instead of optimizing them, but for most applications (as we have here), the marginal likelihood is sharply peaked. Optimization is therefore a good approximation to marginalization, so for the purpose of the model selection we describe in this paper, there is no freedom to choose σ_f and l separately.

2.3 Reconstructed $H(z)$ Function versus the Data

Let us now pause briefly to discuss a very salient point emerging from the reconstructed $H(z)$ functions shown in figures 1 and 2. As alluded to above, cosmic chronometer measurements of the Hubble constant have themselves been used in recent years, primarily to optimize the parameters in the standard model ΛCDM, but also on occasion to compare the predictions of ΛCDM with those of the $R_\mathrm{h} = ct$ universe [7, 8]. In the latter, the power-law form of the expansion rate, i.e., $H(z) = H_0(1+z)$, has been shown to fit these data better than the variable rate in the standard model. But those results were the outcome of model fitting to the data. Figure 1 provides us with a new perspective on this comparison, because the Hubble constant reconstructed from the data using Gaussian Processes is entirely free of any presumed model or assumed fitting function. And this approach clearly demonstrates that the $(1+z)$ power law is a much better representation of the reconstructed $H(z)$ function than the variable rate predicted by the standard model (see fig. 3 below). This outcome should not be underestimated, particularly in view of other recent attempts at showing that the cosmic chronometer data support the inference that the Universe underwent a transition from deceleration to acceleration at a redshift $z \sim 0.5 - 0.7$ [2]. These arguments are based on the adoption of specific empirical functions to fit the data, unlike the Gaussian Process reconstruction which makes no such assumptions. The reconstructed $H(z)$ in figure 1 shows no evidence of such a transition, validating the conclusions drawn earlier in refs. [7, 8]. As we shall see shortly, however, the function $H(z)$ reconstructed from the data with reduced dispersions (fig. 2) is not as compelling as figure 1 in this regard, principally because none of the models fits it as well as in the first case. Nonetheless, the model rankings are not changed, so the two reconstructions agree qualitatively, if not quantitatively.

3 Model Comparisons

In this section, we will now briefly introduce the 6 different cosmological models we intend to test against the reconstructed $H(z)$ functions, including the concordance model (based on the *Planck* optimized parameters) and the $R_\mathrm{h} = ct$ universe. The models we will compare are the following:

1. The $R_\mathrm{h} = ct$ universe (a Friedmann-Robertson-Walker cosmology with zero active mass; [16, 17]). The basis for this model is the total equation of state $\rho + 3p = 0$, where ρ and p are the total energy density and pressure of the cosmic fluid [9, 11, 16, 17]. This cosmology has only one free parameter—the Hubble constant H_0, and

$$H^{R_\mathrm{h}=ct}(z) = H_0(1+z)\ . \tag{3.1}$$

2. The concordance model, based on the *Planck* optimization of the parameters in ΛCDM. This model has the Hubble function

$$H^{\Lambda\mathrm{CDM}}(z) = H_0\left[\Omega_\mathrm{m}(1+z)^3 + \Omega_\mathrm{r}(1+z)^4 + \Omega_\Lambda\right]^{1/2}\ , \tag{3.2}$$

   where Ω_i is the energy density ρ_i of species i, for radiation (Ω_r), matter (Ω_m) and dark energy (Ω_Λ), scaled to the critical density, $\rho_c \equiv 3c^2H_0^2/8\pi G$. Its parameters have the (fixed) prior values $H_0 = 67.4 \pm 1.4$ km s^{-1} Mpc^{-1}, $\Omega_\mathrm{m} = 0.314 \pm 0.020$, and $\Omega_\Lambda = 0.686 \pm 0.020$ [26]. Note that $\Omega_\mathrm{r} \ll 1$ in the redshift range associated with cosmic chronometers, and $\Omega_\mathrm{m} + \Omega_\Lambda$ (with $\Omega_\mathrm{r} = 0$) was fixed to 1 because this parameter optimization represents a flat universe. We therefore do not include a spatial curvature term Ω_k in Equation (3.2).

3. The flat ΛCDM (Ω_m) model, with matter and dark-energy densities fixed by the condition $\Omega_\Lambda = 1 - \Omega_\mathrm{m}$ (when radiation is insignificant). The predictions of this model are based on Equation (3.2) with the optimization of one free parameter, Ω_m.

4. The flat ΛCDM (w) model, with matter and dark-energy densities fixed by the condition $\Omega_\mathrm{de} = 1 - \Omega_\mathrm{m}$ (again, when radiation is insignificant). Here, H_0 and Ω_m have prior values (from *Planck*), but the dark-energy equation of state, $w_\mathrm{de} \equiv p_\mathrm{de}/\rho_\mathrm{de}$, where p_de is the dark-energy pressure, is unconstrained. Also,

$$H^{w\mathrm{CDM}}(z) = H_0\left[\Omega_\mathrm{m}(1+z)^3 + \Omega_\mathrm{r}(1+z)^4 + \Omega_\mathrm{de}(1+z)^{3(1+w_\mathrm{de})}\right]^{1/2}\ . \tag{3.3}$$

5. The flat ΛCDM (H_0) model, with matter and dark-energy densities fixed by the condition $\Omega_\Lambda = 1 - \Omega_\mathrm{m}$ (when radiation is insignificant). Its predictions are based on Equation (3.2) with an unconstrained H_0.

6. Einstein–de Sitter space, which contains only matter. This model has only one free parameter, H_0, and

$$H^{\mathrm{EdS}}(z) = H_0(1+z)^{3/2}\ . \tag{3.4}$$

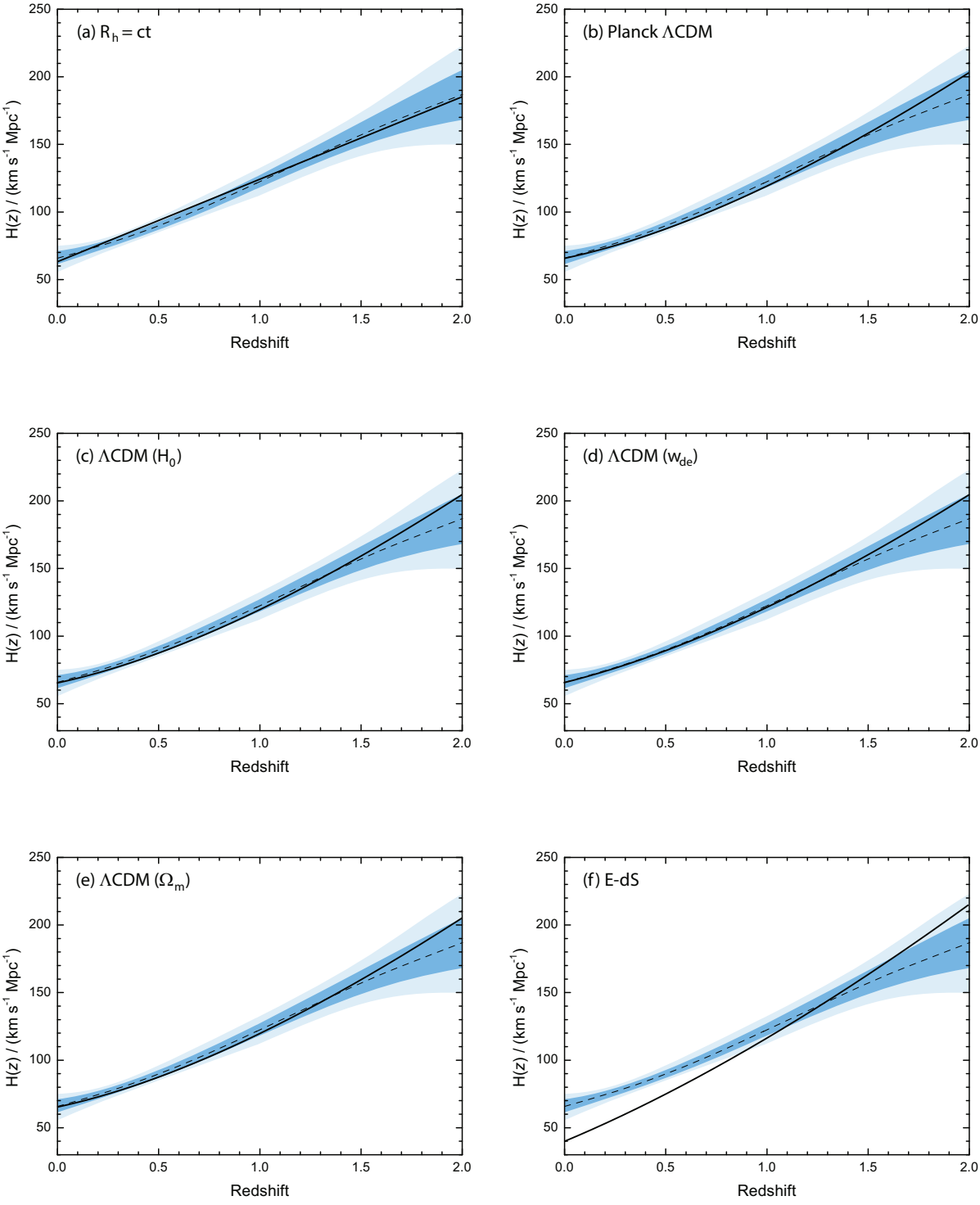

Figure 3. The Hubble constant $H(z)$ (solid curve) in various cosmologies optimized to fit the reconstructed function in figure 1 (dashed curve): (a) The $R_{\rm h} = ct$ universe; (b) Planck ΛCDM; (c) ΛCDM (H_0), with a re-optimized (i.e., re-fitted) Hubble parameter; (d) flat ΛCDM ($w_{\rm de}$); (e) ΛCDM ($\Omega_{\rm m}$); (f) Einstein de Sitter. The blue bands indicate the 1σ (dark shade) and 2σ (light shade) confidence regions from figure 1.

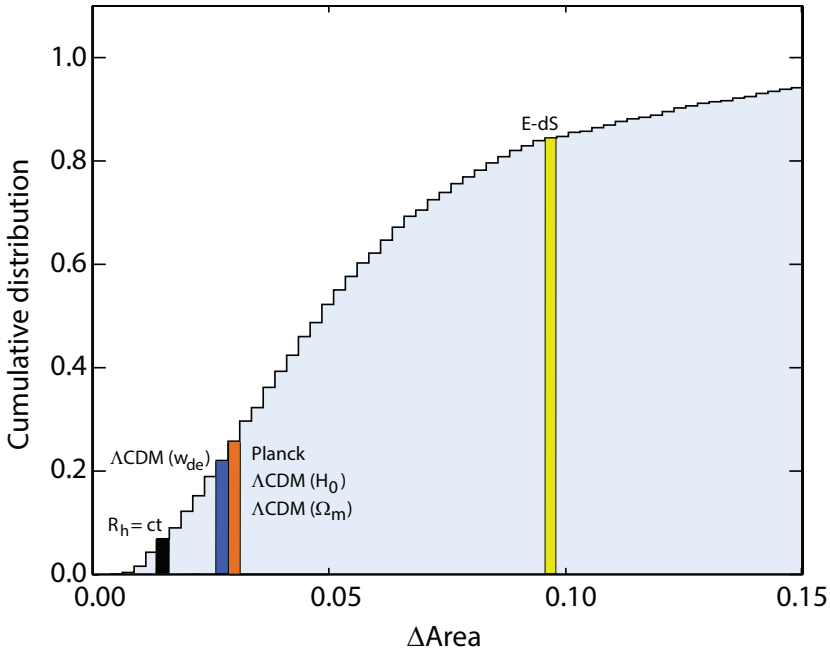

Figure 4. Cumulative probability distribution (normalized to 1) of the differential area calculated for $H(z)$ according to Equation (3.5) for mock samples constructed via Gaussian randomization of the measured $H(z_i)$ values (see text preceding Equation 3.5). The various models are shown according to their probabilities listed in Table 1.

Starting with the $H(z)$ function reconstructed using the full sample of 30 measurements (fig. 1), one may gauge how well it compares to model predictions by examining the theoretical best-fit curves (more on this below) in relation to the 1σ and 2σ confidence regions shown in figure 3. For the sake of clarity, the reconstructed $H(z)$ curve itself is shown as a thin dashed line in these panels. A quick inspection by eye suggests that the $R_{\rm h} = ct$ curve is very close to the reconstructed function, while the other models all have some excess curvature, either at low or high redshifts, introducing at least some tension with the observations.

To quantify these comparisons, we will adopt the following procedure. We use the data and their 1σ errors plotted in figure 1 to create mock samples of 30 values of the Hubble constant with the same redshifts, z_i $(i = 1, ..., 30)$, as the measurements, but with Gaussian randomized values $H^{\rm mock}(z_i) = H(z_i) + r\sigma_i$, where r is a Gaussian random variable with mean 0, and variance 1, and σ_i is the dispersion at z_i (see figure 1).

Using these mock data, we reconstruct a mock $H^{\rm mock}(z)$ function, and then calculate a normalized absolute area difference between this and the real function, according to

$$\Delta A = \int_0^2 dz \, \Big| H^{\rm mock}(z) - H(z) \Big| \Big/ \int_0^2 dz \, H(z) \; . \tag{3.5}$$

With this approach, we build a distribution of frequency versus differential area [27], from which we then construct the cumulative probability distribution shown in figure 4.

For each model i, we calculate the differential areas analogous to Equation (3.5), replacing $H^{\rm mock}$ with its model specific function $H^i(z)$, and then estimate the probability (i.e., the p-value) of this cosmology being consistent with the reconstructed $H(z)$ function using

Table 1. Model comparison using the $H(z)$ function reconstructed from the 30 measurements with published errors. The value of $\Omega_{\rm m}$ is fixed in every case, except for the model ΛCDM ($\Omega_{\rm m}$)

Model	H_0 (km s^{-1} Mpc^{-1})	$\Omega_{\rm m}$	$\Omega_{\rm de}$	$w_{\rm de}$	Prob. (%) (Fig. 4)
$R_{\rm h} = ct$	63.0	–	–	–	93.0
ΛCDM ($w_{\rm de}$)	67.4	0.314 (fixed)	$1 - \Omega_{\rm m}$	-0.913	83.0
ΛCDM (H_0)	70.5	0.314 (fixed)	$1 - \Omega_{\rm m}$	-1	78.3
Planck ΛCDM	67.4	0.314 (fixed)	$1 - \Omega_{\rm m}$	-1	74.2
ΛCDM ($\Omega_{\rm m}$)	67.4	0.314 (optimized)	$1 - \Omega_{\rm m}$	-1	74.2
E-dS	41.3	1.0 (fixed)	–	–	16.6

figure 4. For a given ΔA, this figure shows what fraction of the randomized realizations had a differential area smaller than this value. Thus, a model's calculated ΔA shows the probability (the p-value) that this cosmology's prediction differs from the reconstructed $H(z)$ function due solely to cosmic variance. If a model has a free parameter, we optimize its value within its physically meaningful range by finding a minimum of the differential area ΔA. For $\Omega_{\rm m}$, this range is $(0, 1)$, while for $w_{\rm de}$ we assume $(-1, 0)$, i.e., we exclude phantom dark energy with $w_{\rm de} < -1$. The resulting probabilities and parameter values are quoted in Table 1.

As we expected from a quick inspection of figure 3, the reconstructed Hubble constant prefers the $R_{\rm h} = ct$ cosmology, and provides reasonable fits for ΛCDM with either of the parameters $w_{\rm de}$, H_0 or $\Omega_{\rm m}$ re-optimized to fit the reconstructed $H(z)$ function, but with smaller probabilities. Quite coincidentally, the optimized value of $\Omega_{\rm m}$ when it is the sole parameter allowed to vary (row 5) is identical to the *Planck* value (row 4). As such, the probabilities for Planck ΛCDM and ΛCDM ($\Omega_{\rm m}$) are the same. The Einstein-de Sitter model, however, is strongly disfavoured by this comparative test.

We repeat this procedure using the data with reduced dispersions (fig. 2) in order to gauge the impact of correlation in the systematic errors on the reconstruction of $H(z)$. The individual model fits are shown in figure 5, with the corresponding cumulative probability distribution in figure 6. The model rankings and their probabilities are listed in Table 2. We notice in this case that none of the models fit the reconstructed $H(z)$ function very well. Even $R_{\rm h} = ct$, which is marginally favoured over the others, sits at roughly the halfway point of all possible Gaussian randomizations based on the reduced measurement errors, i.e., a simple variance of the reconstructed function $H(z)$ would produce a differential area ΔA smaller than that corresponding to $R_{\rm h} = ct$ about half of the time. Though the two model rankings (in Tables 1 and 2) are consistent with each other, one can see from figure 2 why the second reconstructed $H(z)$ is not fully consistent with the first. The scatter in the measurements increases with redshift, suggesting that a simple uniform reduction (by 25%) of the errors to account for partial correlation in the systematics may not be a reasonable approach. But attempting a more detailed mitigation of the systematic errors is not feasible, given how little is known at this stage about $\sigma_{\rm stat}$ and, particularly, $\sigma_{\rm sys}$.

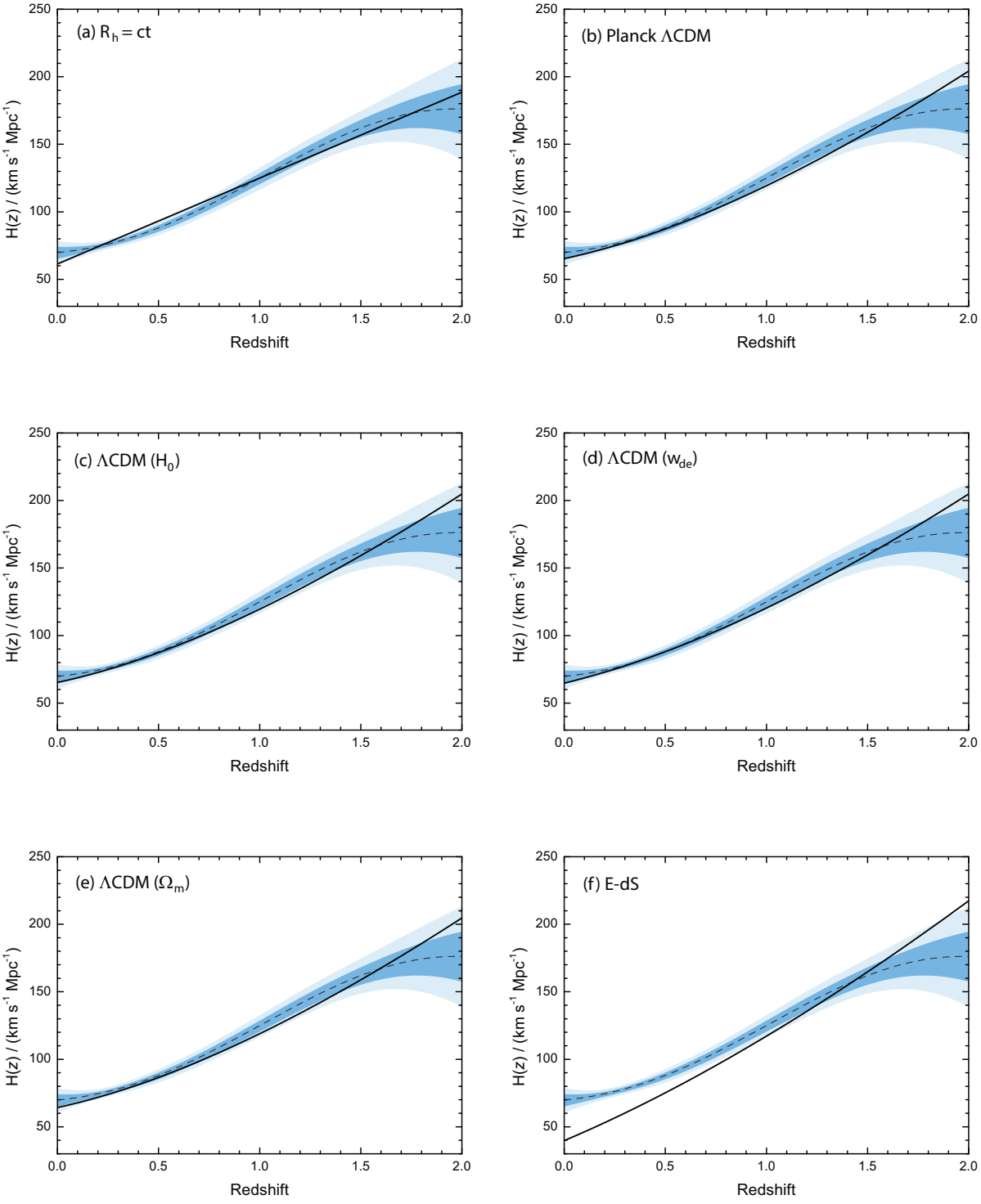

Figure 5. The Hubble constant $H(z)$ (solid curve) in various cosmologies optimized to fit the reconstructed function in figure 2 (dashed curve): (a) The $R_{\rm h} = ct$ universe; (b) Planck ΛCDM; (c) flat ΛCDM (H_0); (d) flat ΛCDM ($w_{\rm de}$); (e) ΛCDM ($\Omega_{\rm m}$); (f) Einstein de Sitter. The blue bands indicate the 1σ (dark shade) and 2σ (light shade) confidence regions from figure 2.

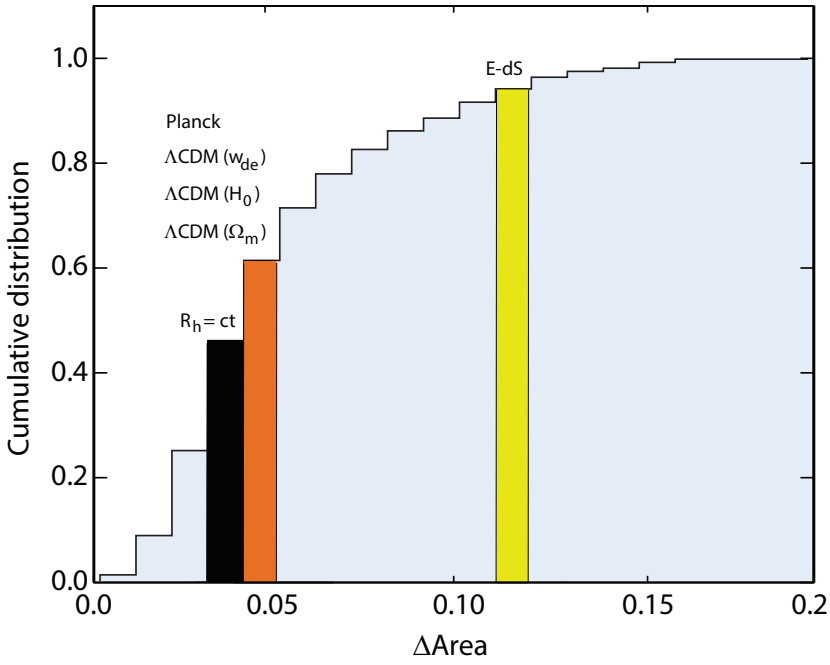

Figure 6. Cumulative distribution (normalized to 1) of the differential area ΔA calculated for $H(z)$ according to Equation (3.5) for mock samples constructed via Gaussian randomization of the (modified) $H(z_i)$ values shown in figure 2. The various models are shown according to their probabilities listed in Table 2.

Table 2. Model comparison based on the reconstructed $H(z)$ with errors artificially reduced by 25%

Model	H_0 (km s^{-1} Mpc^{-1})	$\Omega_{\rm m}$	$\Omega_{\rm de}$	$w_{\rm de}$	Prob. (%) (Fig. 6)
$R_{\rm h} = ct$	62.7	–	–	–	54.7
ΛCDM ($w_{\rm de}$)	67.4	0.314 (fixed)	$1-\Omega_{\rm m}$	-0.94	39.6
ΛCDM (H_0)	68.0	0.314 (fixed)	$1-\Omega_{\rm m}$	-1	39.6
ΛCDM ($\Omega_{\rm m}$)	67.4	0.319 (optimized)	$1-\Omega_{\rm m}$	-1	39.6
Planck	67.4	0.314 (fixed)	$1-\Omega_{\rm m}$	-1	15.2
E-dS	42.0	1.0 (fixed)	–	–	7.3

4 Conclusions

We have used Gaussian Processes to reconstruct the Hubble constant $H(z)$ and its associated 1σ and 2σ confidence regions, based exclusively on the observation of cosmic chronometers. This is an important constraint, given that other methods of measuring the Hubble constant invariably rely on the pre-assumption of a particular cosmological model, which biases any subsequent analysis of the data for the purpose of model selection. For example, using BAO to determine the Hubble constant generally requires the assumption of a fiducial model in

order to separate the cosmological redshift of the BAO peak from effects associated with internal redshift space distortions. This possible contamination arises when the positions of galaxies are plotted in redshift-space rather than in terms of their angular-diameter distance, and is due to the peculiar motion of galaxies subject to their mutual gravitational attraction, contributing a Doppler shift in addition to the cosmological redshift. In order to 'measure' and subtract this Doppler effect, one must adopt a specific expansion scenario. Thus, the inferred BAO scale and $H(z)$ are relevant to that model, but not necessarily to the alternatives. And local measurements of $H(z)$, e.g., using Cepheid variables or other types of distance calibration, are often based on the parametrization in ΛCDM though, in principle, a re-calibration could be made for each individual model. The reconstructed $H(z)$ used in this paper is completely model free, and is therefore suitable for probing the expansion history without any prejudice.

The reconstructed $H(z)$ confirms the results of earlier work [7, 8], which showed that the Hubble constant measured with cosmic chronometers does not support models with a variable expansion rate, preferring instead the constant rate of expansion predicted by the $R_\mathrm{h} = ct$ universe. The earlier results were based on optimizing model fits to the $H(z)$ data. The $H(z)$ function reconstructed with the use of Gaussian Processes is, in principle, arguably better because it is obtained without reference to any model at all. Even a simple comparison by eye of the reconstructed $H(z)$ in figure 1 with the corresponding best fit curves in figure 1 of ref. [12] suggests that the cosmic chronometer data favour a constant expansion rate over a variable one.

The key results of our analysis are summarized in Tables 1 and 2. Of the six models we compared here, the one favoured by the reconstructed $H(z)$—based on both the published measurements (figure 1) and (though to a lesser extent) the data with artificially reduced dispersions (figure 2)—is $R_\mathrm{h} = ct$. ΛCDM and its variations also provide reasonably good fits—at least for $z \ll 2$ (see figs. 3 and 5)—but with smaller p-values. One of the least favoured models is actually the version of ΛCDM with the *Planck* optimization of parameters. It is also important to note that the other versions of ΛCDM explored here were fitted using *Planck* priors on their free parameters, except for one of them that is different in each case, while the $R_\mathrm{h} = ct$ model has only one free parameter (H_0), and no prior was applied to it. Information criteria provide a greater penalty to less parsimonious models (i.e., those using a larger number of free parameters), so a model comparison based, e.g., on the Bayes Information Criterion [28], would have produced an even greater disparity in probabilities than those listed in the tables.

The analysis reported in this paper continues to build the case for the $R_\mathrm{h} = ct$ cosmology. The standard model accounts for the data at both high and low redshifts, but tension between its predictions and the observations grows as the error in the measurements drops to levels of a few percent. This is seen in the angular correlation function of the CMB, in the BAO scale measured with the Ly-α cross-correlation function, and in the growth rate at $z < 1$. In purely technical terms, the chief difference between these two models is that the former has a strictly constant equation of state, corresponding to the zero active mass condition [13, 17], while the latter has an equation of state that varies as the relative abundances of the constituents in the cosmic fluid change with redshift.

One would think that such a difference might produce only subtle changes in the expansion rate and other observable signatures. That may be true in some respects, but definitely not in others. For example, this difference in the equation of state completely eliminates the horizon problem, thereby obviating the need for an early phase of inflated expansion

[29]. Considering how difficult it has been to find a completely satisfactory model of inflation, the $R_{\rm h} = ct$ universe provides an acceptable alternative to the current inflationary ΛCDM paradigm. Such an outcome would bring to an end the 30-year endeavor to fix the horizon problem, which emerged from the initially misunderstood expansion history of the Universe. The observations today suggest a cosmic age consistent with a constant expansion rate since the very beginning. The non-empty $R_{\rm h} = ct$ universe (as opposed to the empty, curvature-driven Milne universe) formally describes this constantly-expanding cosmos, and very interestingly permits all areas of the Universe observable today to have reached thermal equilibrium well before the cosmic microwave background was produced. If correct, the $R_{\rm h} = ct$ describes a much simpler, more elegant cosmos without the pathologies (e.g., the horizon problem) requiring layers of 'fixes' to address apparent inconsistencies between the measurements at high and low redshifts.

Acknowledgments

We are grateful to the anonymous referee for very helpful, detailed comments that have led to a significant improvement in the presentation of our results. Some of this work was carried at the Instituto de Astrofísica de Canarias in Tenerife, and was partially supported by grant 2012T1J0011 from The Chinese Academy of Sciences Visiting Professorships for Senior International Scientists.

References

[1] Jimenez, R. & Loeb, A., "Constraining Cosmological Parameters Based on Relative Galaxy Ages," ApJ, **573**, 37 (2002)

[2] Moresco, M., Pozzetti, L., Cimatti, A., Jimenez, R., Maraston, C., Verde, L., Thomas, D., Citro, A., Tojeiro, R. & Wilkinson, D., "A 6% measurement of the Hubble parameter at $z \sim 0.45$: direct evidence of the epoch of cosmic re-acceleration," JCAP, **05**, id 014 (2016)

[3] Rasmussen, C. & Williams, C., "Gaussian Processes for Machine Learning," Cambridge: The MIT Press (2006)

[4] Holsclaw, T., Alam, U., Sanso, B., Lee, H., Heitmann, K., Habib, S. & Higdon, D., "Nonparametric Dark Energy Reconstruction from Supernova Data," Phys. Rev. Lett., **105**, id 241302 (2010)

[5] Seikel, M., Clarkson, C. & Smith, M., "Reconstruction of dark energy and expansion dynamics using Gaussian processes," JCAP, **06**, 036S (2012)

[6] Moresco, M., Cimatti, A., Jimenez, R. et al., "Improved constraints on the expansion rate of the Universe up to $z \sim 1.1$ from the spectroscopic evolution of cosmic chronometers," JCAP, **8**, id 006 (2012)

[7] Melia F. & Maier, R., "Cosmic Chronometers in the $R_{\rm h} = ct$ Universe," MNRAS, **432**, 2669 (2013)

[8] Melia, F. & McClintock, T. M., "A Test of Cosmological Models Using High-z Measurements of $H(z)$," AJ, **150**, id 119 (2015)

[9] Melia, F., "The Cosmic Horizon," MNRAS, **382**, 1917 (2007)

[10] Melia, F. & Abdelqader, M., "The Cosmological Spacetime," **IJMP-D**, 18, 1889 (2009)

[11] Melia, F. & Shevchuk, A., "The $R_{\rm h} = ct$ Universe," MNRAS, **419**, 2579 (2012)

[12] Wei, J.-J., Melia, F. & Wu, X.-F., "Impact of a Locally Measured H_0 on the Interpretation of Cosmic Chronometer Data," ApJ, **835**, 270 (2017)

[13] Shi X., "Peculiar Hubble Flows in Our Local Universe," ApJ, **486**, 32 (1997)

[14] Keenan, R. C., Barger, A. J. & Cowie, L. L., "Evidence for a ~ 300 Megaparsec Scale Under-density in the Local Galaxy Distribution," ApJ, **775**, 62 (2013)

[15] Romano, A. E., "Hubble trouble or Hubble bubble?" e-print (arXiv:1609.04081) (2017)

[16] Melia, F., "Physical Basis for the Symmetries in the Friedmann-Robertson-Walker Metric," Frontiers of Physics, **11**, 119801 (2016)

[17] Melia, F.,"The Zero Active Mass Condition in Friedmann-Robertson-Walker Cosmologies," Front Phys, **12**, 129802 (2017)

[18] Blake, C. et al., "The WiggleZ Dark Energy Survey: joint measurements of the expansion and growth history at $z < 1$," MNRAS, **425**, 405 (2012)

[19] Treu, T., Ellis, R. S., Liao, T. X., van Dokkum, P. G., Tozzi, P., Coil, A., Newman, J., Cooper, M. C. & Davis, M., "The Assembly History of Field Spheroidals: Evolution of Mass-to-Light Ratios and Signatures of Recent Star Formation," ApJ, **633**, 174 (2005)

[20] Simon, J., Verde, L. & Jimenez, R., "Constraints on the redshift dependence of the dark energy potential," PRD, **71**, id 123001 (2005)

[21] Stern, D., Jimenez, R., Verde, L., Stanford, S. A. & Kamionkowski, M., "Cosmic Chronometers: Constraining the Equation of State of Dark Energy. II. A Spectroscopic Catalog of Red Galaxies in Galaxy Clusters," ApJS, **188**, id 280 (2010)

[22] Zhang, C., Zhang, H., Yuan, S., Liu, S., Zhang, T.-J., Sun & Y.-C., "Four new observational $H(z)$ data from luminous red galaxies in the Sloan Digital Sky Survey data release seven," Res. Astron. Astrophys., **14**, 1221 (2014)

[23] Moresco, M., "Raising the bar: new constraints on the Hubble parameter with cosmic chronometers at $z \sim 2$," MNRAS, **450**, L16 (2015)

[24] Leaf, K. & Melia, F., "Analyzing H(z) data using two-point diagnostics," MNRAS, **470**, 2320 (2017)

[25] López-Corredoira, M., Vazdekis, A., Gutiérrez, C. M. & Castro-Rodríguez, N., A&A, in press (arXiv:1702.00380) (2017)

[26] Planck Collaboration, "Planck 2013 results. XXIII. Isotropy and statistics of the CMB," A&A, **571**, id A23 (2014).

[27] Yennapureddy, M. K. and Melia F., "Reconstruction of the HII Galaxy Hubble Diagram using Gaussian Processes," JCAP, **JCAP11(2017)029**, 029 (2017)

[28] Schwarz, G., "Estimating the Dimension of a Model," Ann. Statist., **6**, 461 (1978)

[29] Melia, F., "The $R_{\rm h} = ct$ universe without inflation," A&A, **553**, id A76 (2013)

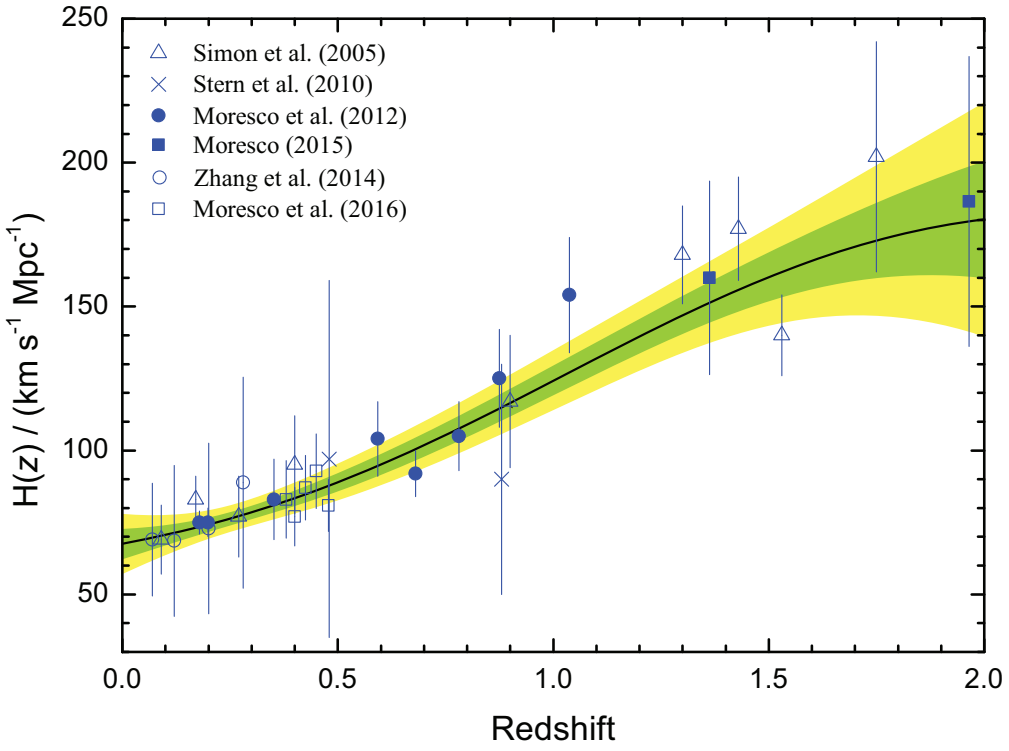

Figure 7. The function $H(z)$ reconstructed with Gaussian Processes (solid black curve), using the Matern92 covariance function (Seikel et al. 2012). The green and yellow shaded regions represent the 1σ and 2σ confidence regions of the reconstruction, respectively.

A Gaussian Processes with an Alternative Covariance Function

The function $H(z)$ representing the 30 cosmic chronometer measurements shown in figure 1 is reconstructed here using a different covariance function $k(x_1, x_2)$ than the 'more conventional' one shown in Equation (2.3). Specifically, we repeat the steps followed in producing figs. 1, 3 and 4, but now with the Matérn covariance function in Gaussian processes, whose explicit form is [5]

$$k(x_1,x_2) = \sigma_f^2 \exp\left(-\frac{3|x_1-x_2|}{l}\right)\left(1+\frac{3|x_1-x_2|}{l}+\frac{27|x_1-x_2|^2}{7l^2}+\right.$$
$$\left.\frac{18|x_1-x_2|^3}{7l^3}+\frac{27|x_1-x_2|^4}{35l^4}\right) . \qquad (A.1)$$

The reconstructed function is shown in figure 7, along with the 30 independent measurements of $H(z)$. This choice of covariance function produces somewhat less smoothing than that using Equation (2.3), with the principal effect of creating greater tension between the predictions of ΛCDM and the data at high redshift, where the standard model requires a more rapid increase in $H(z)$ with z than the reconstruction produces. The model comparisons are made in figure 8, and the corresponding cumulative probabilities are shown in figure 9 and tabulated in Table 3.

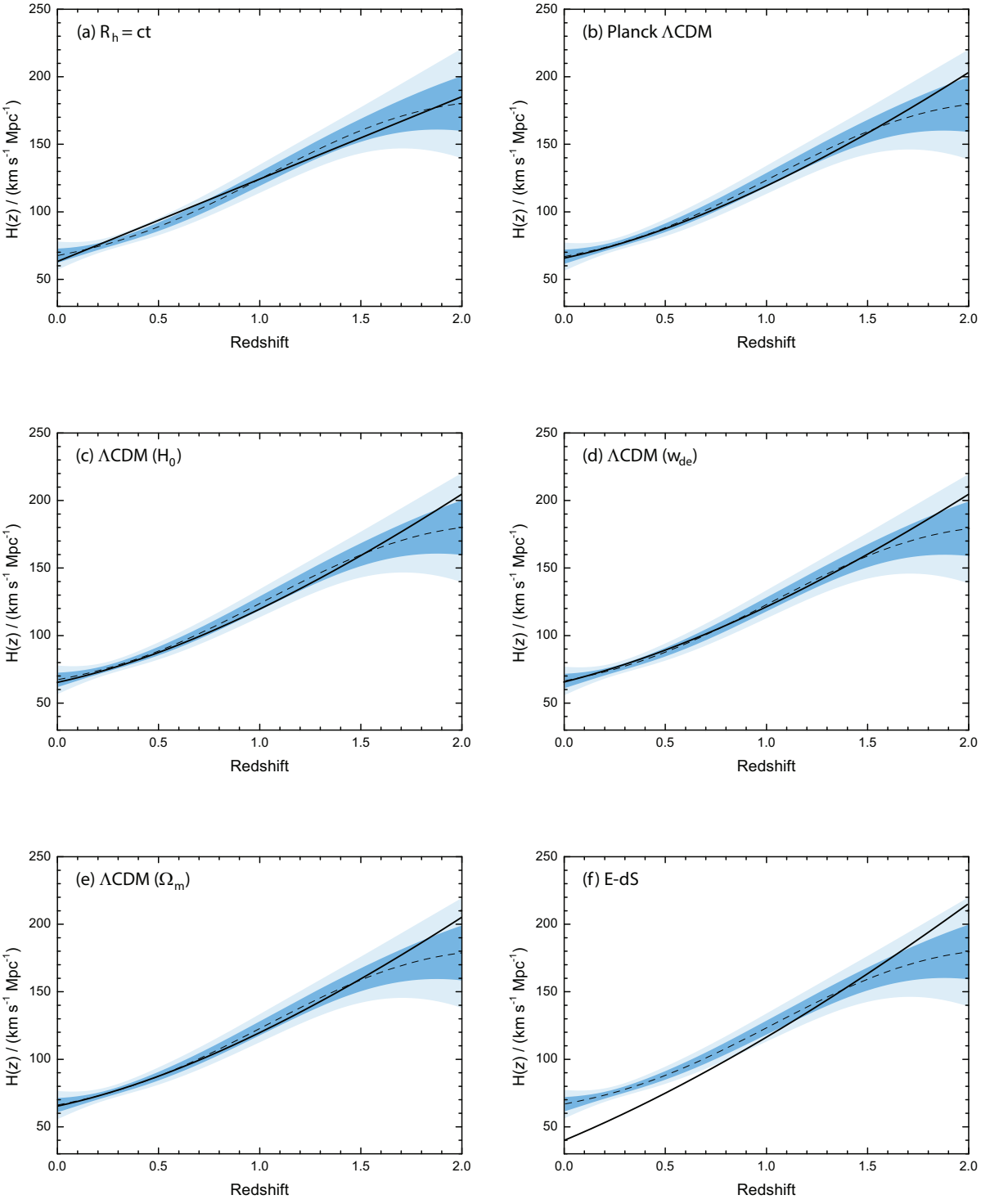

Figure 8. The Hubble constant $H(z)$ (solid curve) in various cosmologies optimized to fit the reconstructed function in figure 7 (dashed shade): (a) The $R_{\rm h} = ct$ universe; (b) Planck ΛCDM; (c) ΛCDM with a prior, $\Omega_{\rm m} = 0.314$; (d) flat ΛCDM, with prior density $\Omega_{\rm m} = 0.314$ and Hubble constant $H_0 = 67.4$ km s^{-1} Mpc^{-1}; and (e) ΛCDM ($\Omega_{\rm m}$); (f) Einstein de Sitter. The blue bands indicate the 1σ (dark shade) and 2σ (light shade) confidence regions from figure 7. See Table 3 for re-optimized parameter values.

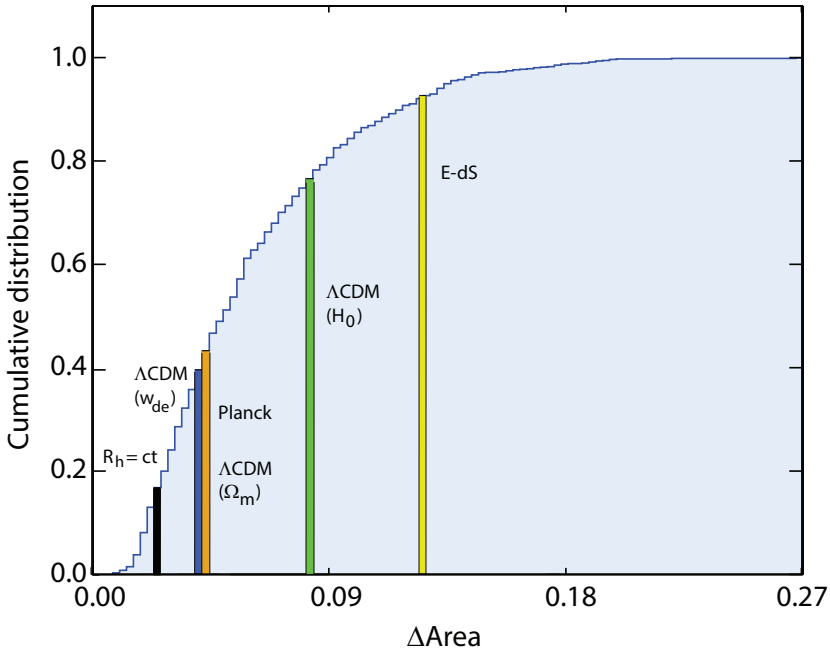

Figure 9. Cumulative probability distribution (normalized to 1) of the differential area calculated for $H(z)$ according to Equation (3.5) for mock samples constructed via Gaussian randomization of the measured $H(z_i)$ values. This calculation is based on the reconstruction shown in figs. 7 and 8, using the Matern92 covariance function (Seikel et al. 2012). The various models are shown according to their probabilities listed in Table 3.

Table 3. Model comparison using a reconstruction with the Matern92 covariance function (Seikel et al. 2012)

Model	H_0 (km s^{-1} Mpc^{-1})	Ω_m	Ω_de	w_de	Prob. (%) (Fig. 9)
$R_\mathrm{h} = ct$	63.0	–	–	–	83.2
ΛCDM (w_de)	67.4	0.314 (fixed)	$1 - \Omega_\mathrm{m}$	−0.913	64.2
Planck ΛCDM	67.4	0.314 (fixed)	$1 - \Omega_\mathrm{m}$	−1	60.4
ΛCDM (Ω_m)	67.4	0.314 (optimized)	$1 - \Omega_\mathrm{m}$	−1	60.4
ΛCDM (H_0)	67.8	0.314 (fixed)	$1 - \Omega_\mathrm{m}$	−1	23.4
E-dS	41.3	1.0 (fixed)	–	–	12.3

A comparison of Tables 1 and 3 shows that the choice of $k(x_1, x_2)$ in Equation (A.1) rather than Equation (2.3) has resulted in slightly different p-values for the various models, but their rank ordering has remained the same. At least for cosmic chronometers, this choice of covariance function in Gaussian Processes does not influence model selection in any meaningful way.